AlCoCrCuFeNi high entropy alloy cluster growth and annealing on silicon: A classical molecular dynamics simulation study.

Lu Xie, Pascal Brault, Anne Lise Thomann, Jean-Marc Bauchire

AlCoCrCuFeNi high entropy alloy cluster growth and annealing on silicon: A classical molecular dynamics simulation study.

Lu Xie, Pascal Brault (*), Anne-Lise Thomann, Jean-Marc Bauchire

GREMI UMR7344 CNRS Université d'Orléans BP6744, 45067 ORLEANS Cedex 2 France

Abstract: Molecular dynamics simulations are carried out for describing deposition and annealing processes of AlCoCrCuFeNi high entropy alloy (HEA) thin films. Deposition results in the growth of HEA clusters. Further annealing between 300K and 1500K leads to a coalescence phenomenon, as described by successive jump in the root mean square displacement of atoms. The simulated X-ray diffraction patterns during annealing reproduces the main feature of the experiments: a phase transition of the cluster structure from bcc to fcc .

(*) Corresponding author: pascal.brault@univ-orleans.fr

Keywords

Molecular dynamics simulation, thin film growth, cluster growth, high entropy alloy, magnetron sputter deposition

1. Introduction

High Entropy Alloys (HEA) are metallic compounds containing 6 to 13 metallic elements in equimolar ratios [1]. In these alloys, because of the high entropy of mixing, formation of brittle intermetallic phases are avoided and multielement solid solutions are rather stabilized (fcc and/or bcc) [2]. The combination of numerous metallic elements with different sizes induces a sluggish atomic diffusion, leading to nanocristalline or amorphous structures. Bulk HEAs have been extensively studied for their excellent properties and performances, including outstanding strength and resistance to oxidation at high temperatures, anti-adhesion, corrosion resistance, high temperature stability, hydrophobicity, high stiffness, strength and toughness, high hardness, superplasticity and high-strain-rate superplasticity [3, 5]. However, HEAs are quite difficult to synthesize as bulk materials because very fast cooling rates are required to avoid formation of mixed cristallized phases and to freeze low ordered structures. For many applications, transferring their exceptional properties to a bare material may be of interest. It is well known that deposition of thin films by magnetron sputtering technique takes place in non-equilibrium conditions. When performed on unheated substrates, synthesis of metastable low ordered structures are promoted. Few studies on HEA thin films deposited by magnetron sputtering have been published [6-12] starting from alloyed targets formed by melting or casting, or from mosaic ones [11, 12]. HEAs can be viewed as atomic-scale composites; their final properties come from 1) the combination of the properties of their constituting elements and 2) the stabilized solid solutions and structures. Thus for the design of new alloys dedicated to a given application, prediction of structural features of the thin film would be of particular interest. Understanding the growth mode of such complex multielement films remains a challenging research topic. In this view, carrying out simulation of the process at the atomic level supported by the available literature on metallic alloy thin film growth is of great interest.

The present study is concerned by molecular dynamics (MD) simulation for studying growth and thermal stability, in the range 300-1500 K, of a HEA thin film. The HEA chosen as a reference has already been studied by many groups [3, 5, 7, 8]; it contains an equal molar ratio of Al, Co, Cr, Cu, Fe and Ni. We numerically investigated the deposition of this alloy on Silicon (100) substrates in operating conditions corresponding to that of magnetron sputter deposition method. The Al-Cr-Co-Cu-Fe-Ni interactions are modelled with the Embedded Atom Method (EAM) force field, the Si-Si interaction with the Tersoff potential. The Si-(AlCoCrCuFeNi) interactions are modeled with Lennard-Jones (12-6) potential. The film morphologies and structures are studied by calculating the radial distribution function (RDF) and the X ray diffraction (XRD) patterns. Comparison with available experimental data confirms the interest of MD simulations to predict HEA thin film features [12].

2. Simulation details

MD is a simulation technique for computing the equilibrium and transport properties of a classical many-body system. Giving an initial set of positions and velocities of a system of N atoms, each atom is treated as a point mass, and the atomic motion is based on Newton's equations.

The MD package LAMMPS [13] is used to simulate the deposition of atoms. A script driving the LAMMPS code was written for automating the deposition and the relaxation of the system. MD simulation was carried out in a three dimensional cell, which was periodic only along x and y directions. The substrate is Silicon (100) with dimensions (100×100×20) Å. The deepest two layers of the substrate are fixed, while the other layers are temperature -controlled by mean of a Berendsen thermostat [14].

When an atom is deposited, the system is in a non-equilibrium state. The high energy of the deposited metal atoms can be dissipated with the Berendsen thermostat to keep the whole

temperature around 300K (room temperature) corresponding to the stated value.

Each atom is placed in the vacuum slab at a random position from 5 to 7Å above the surface. The velocities of the deposited atoms are sampled from a Maxwell-Gaussian distribution with a most probable energy of 1 eV, and with randomly selected incident angles. This mean energy corresponds to sputter deposition experimental conditions for 1 Pa argon gas pressure and 10 cm substrate to target distance. The time-step is chosen to be 1fs and each atom is released each 2000 time-steps, i.e. 2 ps. The vapour composition is taken equal to equimolarity. The thin film is shown to exhibit nearly equimolar composition, indicating that sticking coefficients of all elements are close to each others.

For describing the interaction between Al-Co-Cr-Cu-Ni-Fe, we use EAM potential [15, 16]. Such a potential is non-pairwise in the sense that it is based on concepts from density functional theory, which stipulate in general that the energy of a solid is a unique function of the electron density.

In this frame, the total EAM energy E can be expressed as [15, 16]:

$$E_{pot} = \sum_{i=1}^{N} E_i = \frac{1}{2} \sum_{i=1}^{N} \sum_{i,j,i \neq j}^{N} \phi_{ij}(r_{ij}) + \sum_{i=1}^{N} F_i(\rho_i)$$

where E_i is the potential energy of an atom i, $\phi(r_{ij})$ is the pair energy term defined as a function of the interatomic distance r_{ij} between atoms i and j, and $F_i(\rho_i)$ is the many body embedding energy term defined as a function of the local electron density, ρ_i, at the position of atom i. The local electron density is calculated as a linear sum of the partial electron density contributions from the neighboring atoms,

$$\rho = \sum_{j,j \neq 1}^{N} f_i(r_{ij})$$

Where $f_j(r_{ij})$ is the contribution from atom j to the electron density at the site of the atom i.

The pair energy term is defined as:

$$\phi(r) = \frac{A\exp\left[-\alpha\left(\frac{r}{r_e}-1\right)\right]}{1+\left(\frac{r}{r_e}-\kappa\right)^{20}} - \frac{B\exp\left[-\beta\left(\frac{r}{r_e}-1\right)\right]}{1+\left(\frac{r}{r_e}-\kappa\right)^{20}}$$

Where r_e is the equilibrium spacing between nearest neighbors, A, B, α, and β are four adjustable parameters, and κ and λ are two additional parameters for the cutoff. The electron density function is taken with the same form as the attractive term in the pair potential with the same values of β and λ.

The electron density function is:

$$f(r) = \frac{f_e\exp\left[-\beta\left(\frac{r}{r_e}-1\right)\right]}{1+\left(\frac{r}{r_e}-\lambda\right)^{20}}$$

The pair potential between different species a and b is then constructed as:

$$\phi^{ab}(r) = \frac{1}{2}\left[\frac{f^b(r)}{f^a(r)}\phi^{aa}(r) + \frac{f^a(r)}{f^b(r)}\phi^{bb}(r)\right]$$

And the embedding energy function is represented by three equations defining the function in different electron density ranges and having matching values and slopes at the two junctions,

$$F(\rho) = \sum_{i=0}^{3} F_{ni}\left(\frac{\rho}{0.85\rho_e}-1\right)^i, \quad \rho < 0.85\rho_e$$

$$F(\rho) = \sum_{i=0}^{3} F_i\left(\frac{\rho}{\rho_e}-1\right)^i, \quad 0.85\rho_e \le \rho < 1.15\rho_e$$

$$F(\rho) = F_n\left[1-\eta\ln\left(\frac{\rho}{\rho_s}\right)\right]\left(\frac{\rho}{\rho_s}\right)^{\eta}, \quad \rho \ge 1.15\rho_e$$

Where F_{ni}, F_i, and F_n are tabulated constants [15, 16]

Silicon Tersoff empirical potential is used for describing the interaction between Si-Si. This potential has been successfully used to investigate the structural, thermal vibration and surface properties of Si [17,18].

The Tersoff interatomic potential involves both two- and three-body terms:

$$E = \sum_i V_{ij}$$

$$\text{where } V_{ij} = f_C(r_{ij})[f_R(r_{ij}) + b_{ij} f_A(r_{ij})]$$

Here i and j are labels for the atoms. The term with f_A represents a repulsive pair potential due to electron overlap, while f_R represents an attractive pair potential associated with bonding. The function f_C is a smooth cutoff function which limits the range of the potential. The coefficient b_{ij} (bond order) corresponds to a many-body interaction of the form:

$$b_{ij} = \chi_{ij}\left(1 + \beta_i^{n_i} \xi_{ij}^{n_i}\right)^{-1/2n_i}$$

with $\xi_{ij}^{n_i} = \sum_{k \neq i,j} f_C(r_{ik}) g(\theta_{ijk})$ characterising the bond order, with:

$$g(\theta_{ijk}) = 1 + \frac{c_i^2}{d_i^2} - \frac{c_i^2}{d_i^2 + (h_i - \cos\theta_{ijk})^2},$$

the constants χ_{ij}, β_i, n_i, c_i, d_i and h_i depending on the atomic species and θ_{ijk} is the angle between an ij bond and an ik bond.

We use a Lennard-Jones potential for the interactions for Si interactions with Al, Co, Cr, Cu, Fe, Ni) [17]:

$$V_{ij}(r_{ij}) = 4\varepsilon\left[\left(\frac{\sigma}{r_{ij}}\right)^{12} - \left(\frac{\sigma}{r_{ij}}\right)^{6}\right]$$

The parameters ε and σ of Al, Co, Cr, Cu, Fe, Ni and Si LJ potentials are summarized in table 1 [17,19, 20]. σ is the distance at which the LJ potential $V_{ij}(\sigma) = 0$ and -ε is the well depth of the LJ potential.

Table 1: *LJ potential parameters σ and ε for Al, Co, Cr, Cu, Fe, Ni and Si*

Species	ε(eV)	σ(Å)
Al	0.392	2.620
Co	0.510	2.306
Cr	0.502	2.336
Cu	0.409	2.338
Fe	0.527	2.321
Ni	0.520	2.282
Si	0.0175	3.826

While pair potential parameters for these compound materials are not directly available, the Lorenz-Berthelot mixing rule is used for species i and j, giving: $\varepsilon_{ij} = (\varepsilon_i\varepsilon_j)^{1/2}$ and $\sigma_{ij} = (\sigma_i+\sigma_j)/2$ [17]. The use of LJ potentials can be considered as a first attempt for comparison with experiments. Calculating exact Si-metal potentials using ab-initio methods is out of the scope of the present study.

After simulating AlCoCrCuFeNi deposition, the RDF is calculated for determining the average structure. The radial distribution function can be expressed as:

$$\mathbf{g(r)} = \frac{\mathbf{n(r)}}{\rho.4\pi\mathbf{r}^2\Delta\mathbf{r}}$$

Where **g(r)** is the RDF, **n(r)** is the mean number of atoms in a shell of Δ**r** at distance **r**, ρ is the mean atom density. Finally, the simulation of XRDs was also employed to analyze the crystal phases of AlCoCrCuFeNi high-entropy alloy to directly compare with the experimental data. In most radiation scattering experiments, the objective is to obtain information that characterizes either intramolecular or intermolecular structure. In such cases, variation of the scattered intensity with angle is the quantity of main interest, whereas the absolute intensity is of no concern. Thus, ignoring all intensity scale factors and correction factors appropriate for the geometry of the scattering apparatus, the amplitude and intensity of radiation scattered coherently from an arbitrary set of n atoms may be written as:

$$F(\mathbf{Q}) = \sum_{j=1}^{n} f_i \exp(\mathbf{Q}.\mathbf{r_j})$$

$$I(Q) = F(\mathbf{Q}) * F(\mathbf{Q}) = \sum_{j=1}^{n}\sum_{k=1}^{n} f_i f_k \cos(i\mathbf{Q}.\mathbf{r}_{jk})$$

$$Q = \frac{2\pi}{d} = \frac{4\pi \sin\theta}{\lambda}$$

$$\mathrm{f_i} = \int \rho_i \mathbf{r} \exp(-2\pi i \mathbf{Q}\mathbf{r}) \mathrm{d}^3\mathbf{r}$$

Where ρ is the density of atom i, r is the position vector, i is the complex unit and **Q** is the scattering vector (Bragg's Law), f is the atomic scattering factor for the radiation used, and $\mathbf{r}_{jk}$ denotes the vector connecting atoms j and k.

3. Results and discussion.

10000 atoms are released towards the Si(100) surface, for realizing the deposition of equimolar HEA thin films. A random number ζ is generated for selecting the nature of the atom to be released. Al is chosen if $0 \leq \zeta < 1/6$, Co if $1/6 \leq \zeta < 2/6$, and soon. This means 1666 atoms of each kind of element are launched. Table 1 gives the number of atoms really living on the surface. The total number of deposited atoms is 7716, leading to a total sticking coefficient close to 0.80.

Table 2– *Simulated deposited alloy composition*

Atoms	Al	Co	Cu	Cr	Fe	Ni
Deposited atom number	1251	1289	1254	1307	1298	1317
Sticking coefficient	0.751	0.774	0.753	0.785	0.779	0.791
Calculated atomic ratio (ζ)	16.2%	16.7%	16.3%	16.9%	16.8%	17.1%

The final composition is thus $Al_{16.2}Co_{16.7}Cu_{16.3}Cr_{16.9}Fe_{16.8}Ni_{17.1,}$ which is close to equimolarity: theoretical ratio should be 16.67. The final configuration of the grown HEA clusters is shown

in figure 1.

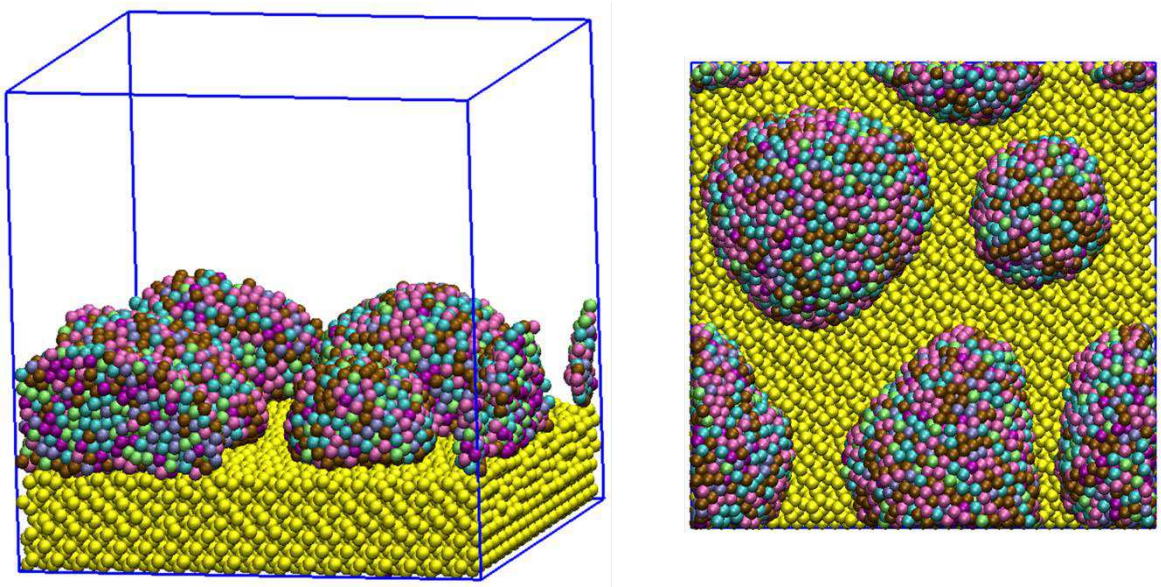

Figure 1*- Side and top views of snapshot of the simulated deposited HEA film. ●Al, ●Co, ●Cr, ●Cu, ●Fe, ●Ni, ●Si*

The film grows as clusters of various sizes in the range 25 – 50 Å. Due to the limited number of impinging atoms (10000) a continuous film is not reached. Nevertheless, this brings the opportunity to explore the behavior under annealing of this cluster assembly.

Once HEA thin film was deposited on the (100) surface of Silicon substrate, the annealing simulation was started. The bottom two layers of the substrate remain fixed as for the deposition step, while the others as well as the supported HEA clusters are temperature-controlled from 300K to 1500K). The important parameter is the temperature increase rate. Two methods are used numerically to carry out the annealing process: first, the temperature was linearly increased from 300K to 1500K at the rate of 2K/ps, 1K/ps, 1K/3ps and 1K/4ps. In the second method, the temperature is first increased at the rate of 1K/3ps, 1K/ps or 2K/ps respectively in a 50K temperature range, then relaxation takes place at the reached temperature for 10^4 time steps (10 ps). This cycle is repeated until the final temperature of 1500 K is reached.

The resulting root mean square displacements (RMSD) at these different rates with the two methods are plotted in figure 2 and 3. Its is seen on Fig. 2 that the RMSD evolves when the annealing rate decreases from 2K/ps down to 1K/3ps. This is due to the fact that the system does not have enough time to relax at the highest annealing rates. However, at a rate 1K/4ps, the lowest one, no further changes of the RMSD are observed. It means that further decreasing the annealing rate, i.e. increasing the time to reach the targeted temperature, does not change the cluster dynamics. Besides, by comparing with the second annealing method, we found that the RMSD at the linear rate of 1K/4ps in figure 2 is essentially the same as for the cycle of 1K/3ps followed by a 10 ps relaxation time (figure 4). So using a slow enough linear rate is comparable to successive cycles including a similar rate followed by a thermal relaxation period.

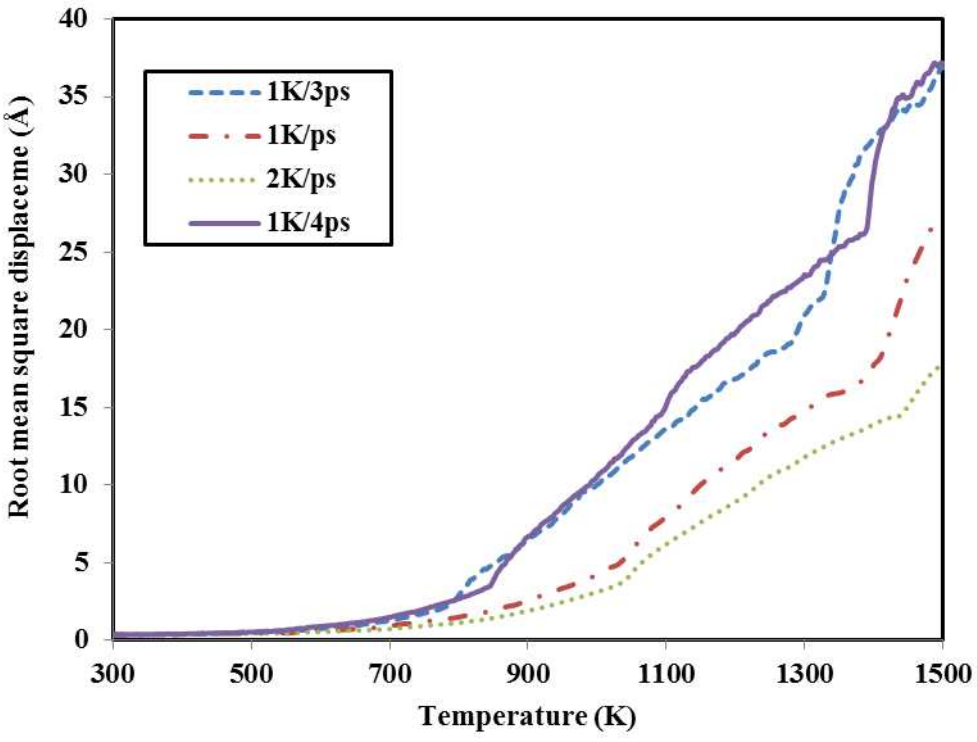

Figure 2 *- Evolution of the total root mean square displacement against the temperature at various annealing rates*

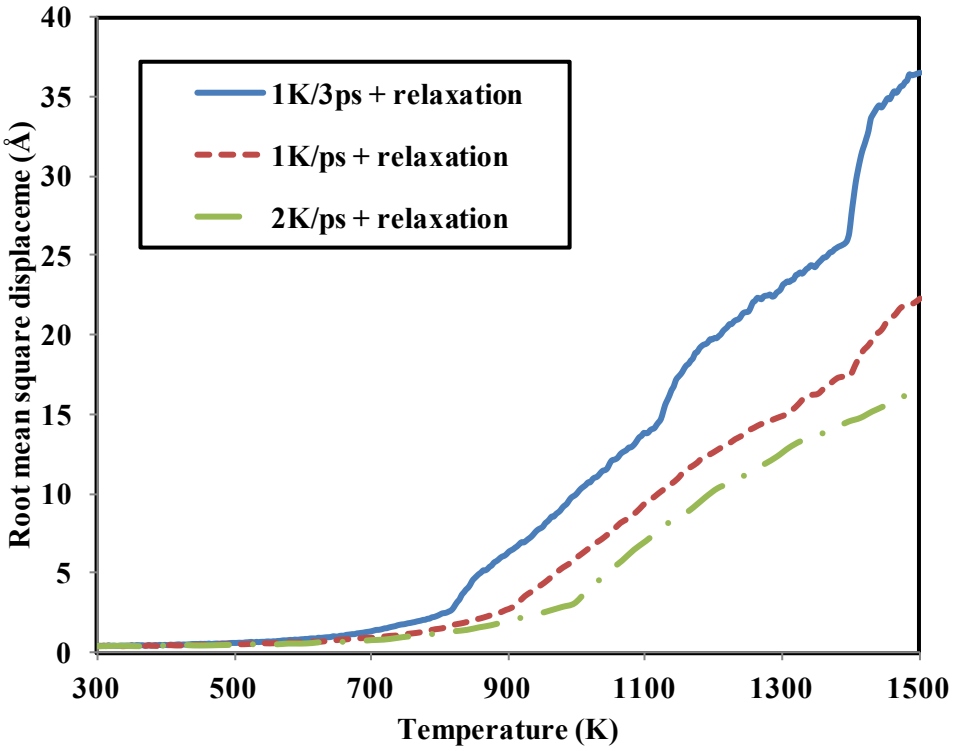

Figure 3 *- Evolution of the total root mean square displacement against the temperature with second annealing method at various annealing rates*

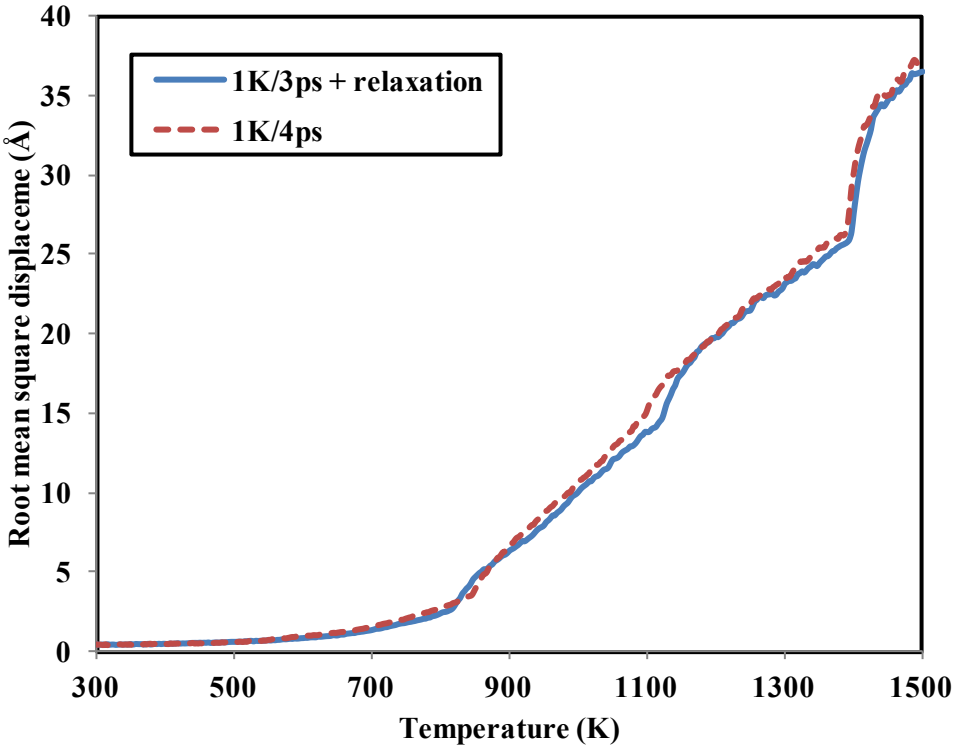

Figure 4 *– The comparison of the total root mean square displacement against the temperature between the two annealing methods at the lowest annealing rates.*

Examination of the snapshot top views, as displayed in figure 5, at different temperature shows a coalescence phenomenon due to temperature induced mobility. The first step is the first coalescence of two clusters (figure 5, images at 850K) which corresponds to the beginning of the jump in the RMSD from 850K to 1095K (figure 4, 1K/4ps). As temperature increases from 1095K to 1395 K, another phenomenon of coalescence is observed involving earlier formed big cluster and a third one. When the temperature is increased up to 1395 K, there is diffusion of the surface atoms leading to the coalescence of all the clusters on the surface (figure 5, image at 1395 and 1500K). At 1395 K, RMSD displays a larger vertical jump in the RMSD.

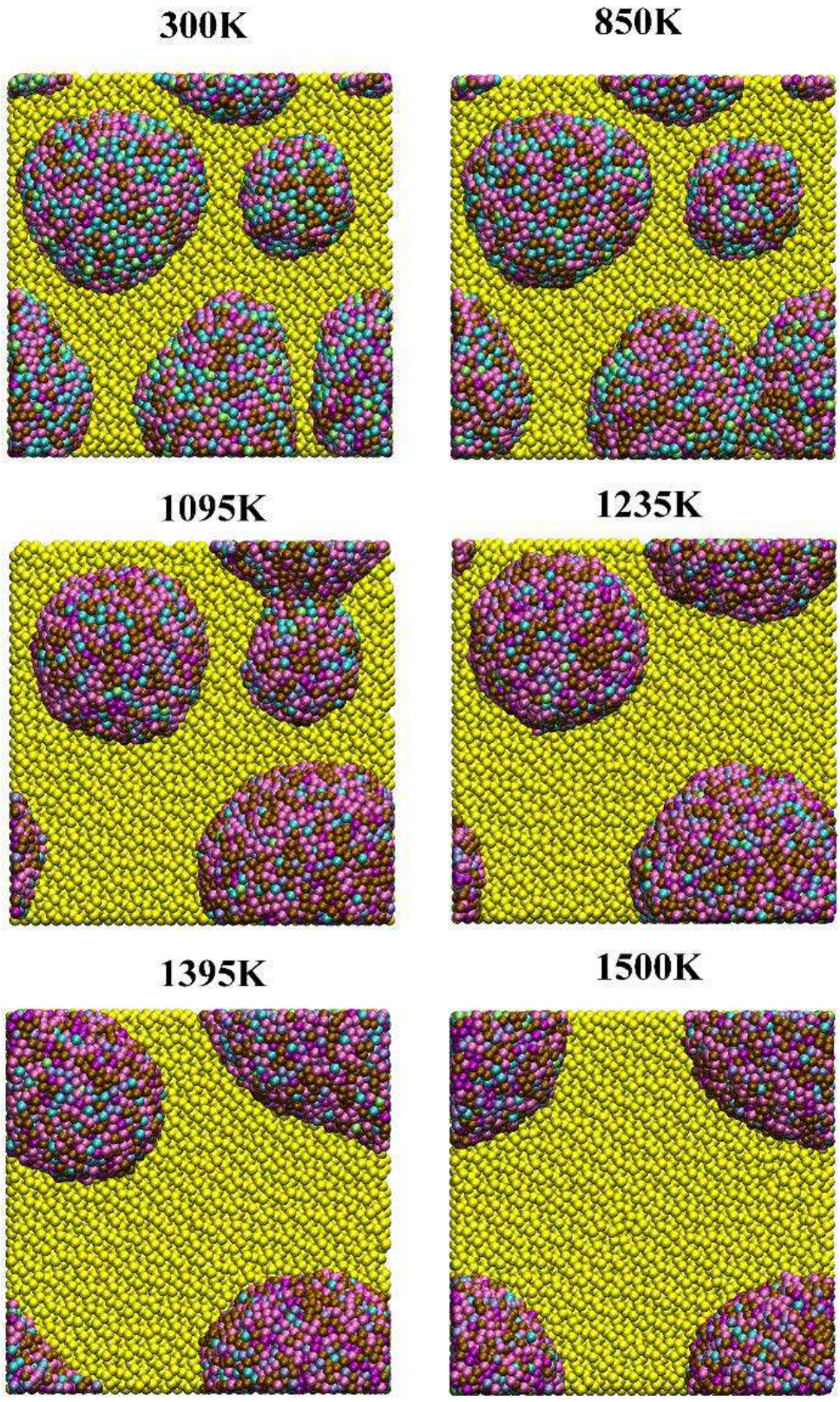

Figure 5 *- Successive snapshots of simulated annealing process (1K/4ps) at different temperatures.* ●*Al,* ●Co, ●Cr, ●Cu, ●Fe, ●Ni, ●Si.

The magnitude of cluster atom motion rises when increasing the temperature. This can be

observed on figure 6 which displays the typical trajectory of an atom, here Fe. Between 300 and 850K, the atom is locally moving: displacements are small and a small domain is visited. Around 850K, there is a small jump and localized displacements with a slightly larger magnitude takes place up to 1095K. Between 1095 and 1235 K, the travelled distance continues to grow up but the motion remains localized. Above 1235 K, the atom has larger displacements and between 1235 and 1395 K the local character is lost. Above 1395 K the atom makes larger displacements and a domain cannot be easily defined: there is a quick motion of the atoms. It behaves like in a fluid, indicating that the cluster is starting to melt.

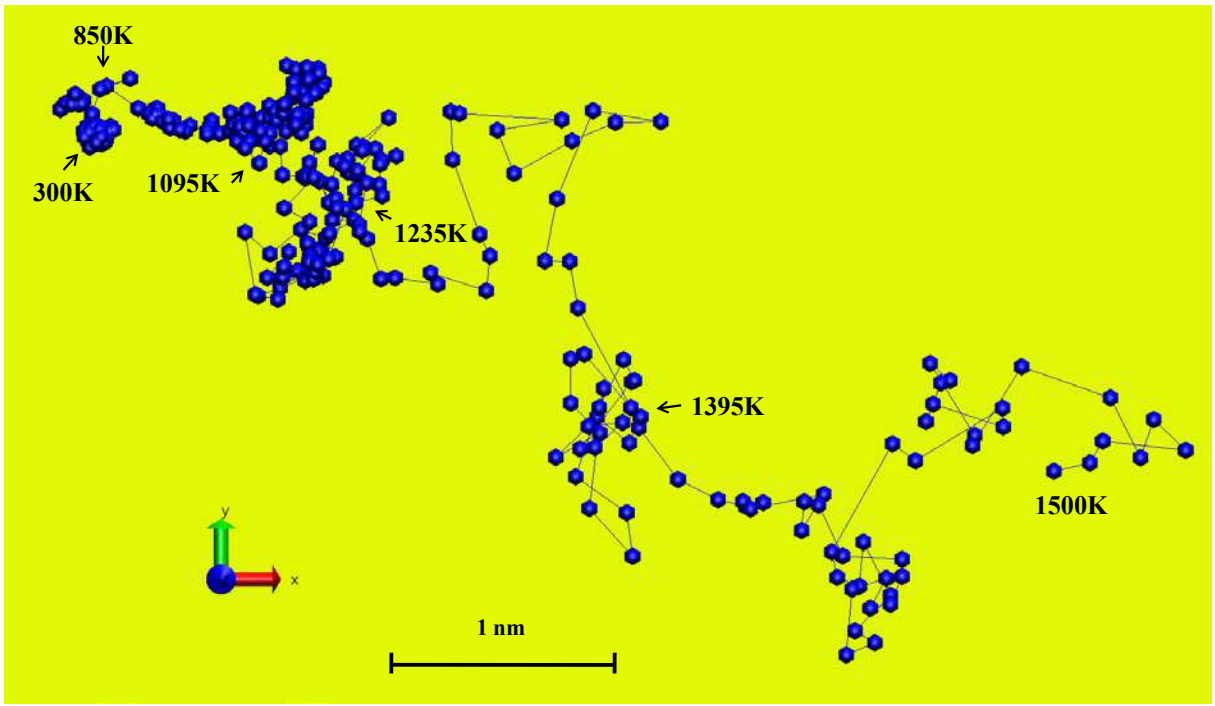

Figure 6 *- Trajectory of typical Fe atom during annealing. Each point of the trajectory is separated by 2.5 K i.e.10 ps.*

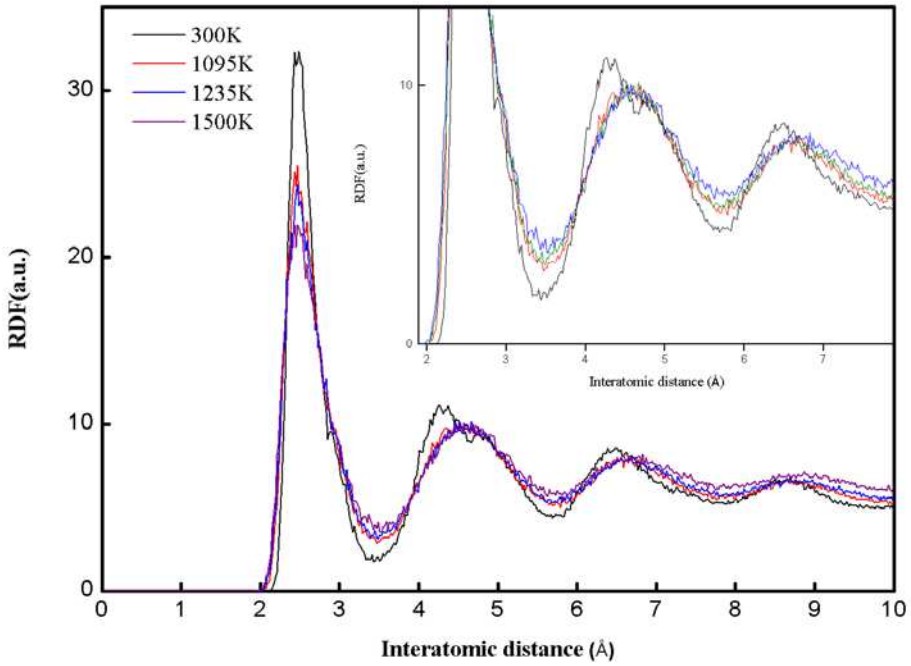

Figure 7 *- Total RDF of the HEA deposit at different annealing temperatures.*

The total RDF is plotted in figure 7 for four temperatures: 300, 1095, 1235, and 1500 K. The peaks represent the successive neighbor distances in the deposited film. This can be compared with the averaged values determined from the features of pure element crystalline phases (see table 3).

Table 3 - *Average neighbour distances in the HEA compared to element crystal values.*

Elements	Lattice parameter (Å)	1st neighbour (Å)	2nd neighbour (Å)	3rd neighbour (Å)	4th neighbour (Å)
Al (fcc)	a_{Al}= 4.05	$\frac{a_{Al}}{\sqrt{2}}$ = 2.86	a_{Al} = 4.05	$\sqrt{\frac{3}{2}}\,a_{Al}$= 4.96	$\sqrt{2}\,a_{Al}$= 5.73
Co (hcp)	a_{Co} = 2.51 c_{Co} = 4.07	a_{Co} = 2.51	$\sqrt{2}\,a_{Co}$ = 3.09	c_{Co} = 4.07	$\sqrt{2}\,c_{Co}$ = 5.76
Cu (fcc)	a_{Cu}= 3.61	$\frac{a_{Cu}}{\sqrt{2}}$ = 2.55	a_{Cu} = 3.61	$\sqrt{\frac{3}{2}}\,a_{Cu}$= 4.42	$\sqrt{2}\,a_{Cu}$= 5.10
Cr (bcc)	a_{Cr} = 2.88	$\frac{\sqrt{3}}{2}a_{Cr}$= 2.49	a_{Cr} = 2.88	$\sqrt{2}\,a_{Cr}$ = 4.07	$\sqrt{\frac{11}{4}}\,a_{Cr}$ = 4.78
Fe (bcc)	a_{Fe} = 2.87	$\frac{\sqrt{3}}{2}a_{Fe}$=	A_{Fe} = 2.87	$\sqrt{2}\,a_{Fe}$ = 4.06	$\sqrt{\frac{11}{4}}\,a_{Fe}$ = 4.76

		2.49			
Ni (fcc)	a_{Ni}= 3.52	$\frac{a_{Ni}}{\sqrt{2}}$ = 2.49	a_{Ni} = 3.52	$\sqrt{\frac{3}{2}}\, a_{Ni}$= 4.31	$\sqrt{2}\, a_{Ni}$= 4.98
Average	-	2.56	3.34	4.32	5.19
HEA T = 300 K	-	2.47	-	4.32	4.81
HEA T = 1095 K	-	2.47	-	-	4.60
HEA T = 1235 K	-	2.47	-	-	4.62
HEA T = 1500 K	-	2.467	-	-	4.61

As can been seen in table 3, nearest neighbor distances of the HEA are different from the element ones and from averaged values calculated for an equimolar stoichiometry. The most important difference is the disappearance of the expected 2nd neighbor distance. This can be explained by recalling that 2ndneighbors in pure crystal structures are located in the neighboring plane. In the monoatomic case, this ordered layer growth only occurs on flat substrate. On atomically disordered surfaces, there is no expected 2nd neighbor [21]. Lack of this peak should be representative of some disorder preventing stacking order to grow. Moreover the slightly different atomic sizes can also contribute to prevent ordered stacking of parallel layers as in the perfect crystal. Moreover this is consistent with the hard ball model [22] addressing the effect of mixing numerous elements with different atomic sizes. Because our systems are compact, the first shell of neighbor atoms will be stable or will only change a little bit due to the presence of neighbor atoms with different atom radius. However the second and third shells are indistinguishable because of the large fluctuation in occupation of different sites. This introduces the disappearance of the second peak in RDFs, too.

We also observe that increasing the temperature leads to the collapsing of 3rd and 4th peaks into a single one.

As the RDF gives the number of atoms located at a given distance, the global analysis of figure 7 shows that the intensity of the first neighbor peak is lowered when increasing

temperature and the tail at long distances is higher for temperatures greater than 850 K. This is also consistent with the increase of RMSD above 850 K. Increasing atom number located at larger interatomic distances means that the correlation distance is increased as in a more fluid state.

Examination of table 3 shows that interatomic distances are contracted, whatever the temperature is, as compared to the average values of the bulk states of the elements. Only the 1st peak is unchanged during annealing and lies below the average bulk value. We cannot thus attribute the peak positions to the effect of specific elements.

A further insight can be achieved by calculating the XRD patterns at different annealing temperatures. Figure 8 displays the evolution of the calculated HEA patterns.

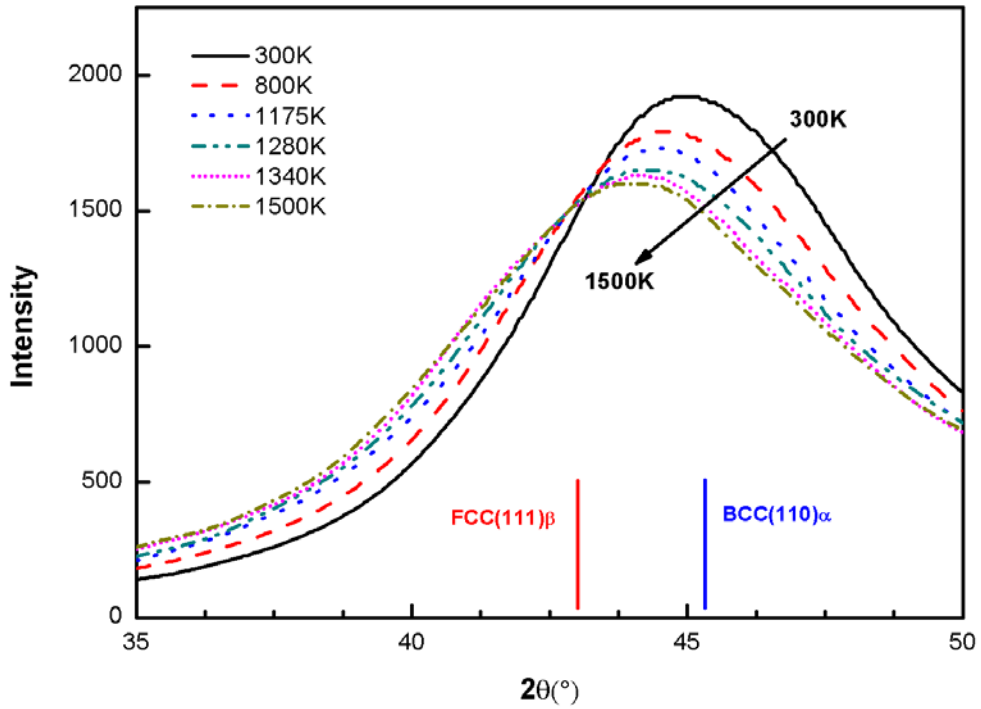

Figure 8 *- The simulated XRD patterns at different annealing temperatures. The two tags at 43 and 45° refer to the experimentally observed fcc and bcc peak values [3].*

It can be observed that the peak position 2θ is shifted from 45° at 300K to 44° at 1500K. In ref. [12], the XRD patterns are found twofold at 300K: one small peak at 42.8° attributed to the fcc(111)β solid solution which coexists with a larger one located at 44.8° attributed to the

bcc(110)α one. When increasing the temperature, experiment shows that the fcc peak increases in magnitude at the expense of the bcc one and moves to lower position: 43° at 1100 K, with complete disappearance of the bcc(110)α peak. Our simulated XRD patterns are consistent with these results: even if, the peak is too large for being resolved as a two XRD peak pattern, the shift towards lower values of simulated peak positions indicates the same trend of phase evolution when increasing annealing temperature, i.e. bcc towards fcc. It is difficult to have more resolution on the simulated XRD pattern due to the small sized layer/clusters, which gives rise to broad peaks. The estimated fcc lattice parameter from the present MD simulations is 3.64 Å and the bcc one is 2.86 Å (see table 4), which compares very well with both experiment (3.66 Å and 2.86 Å, respectively) [12] and bulk calculations (3.60 Å and 2.87 Å, respectively) [23, 24]. The mean cluster size issued from MD simulations is around 25 Å at 300K and 50 Å at 1340K. This is enough for obtaining an XRD pattern, but not for separating fcc and bcc peaks, which are experimentally observed on thick layers (500 nm behing the capabilities of MD simulations).

***Table 4**- Experimental and calculated lattice parameters a. $2d_{hkl} \sin(\theta) = \lambda$ (1.54 Å) and $d_{hkl} = \frac{a}{\sqrt{h^2+k^2+l^2}}$.*

Lattice parameters a	Bulk (calculated) [4, 5]	Experiment thin films [3]	Present work
fcc phase	3.60 Å	300 K 3.66 Å 1100 K 3.64 Å	300 K 3.64 Å
bcc phase	2.86 Å	300 K 2.86 Å 1100 K none	1100 K 2.89 Å

Conclusions

MD simulations are carried out for describing initial growth of HEA thin films. MD simulation reports growth of clusters which evolve during an annealing step from 300K to 1500K. An induced cluster coalescence is observed. This is starting around 850 K where individual atoms are moving inside cluster leading to a first jump in the total RMSD. A larger

jump occurs around 1400K consistent with a melted phase. Moreover XRD calculations at different annealing temperatures show the transition between HEA bcc phase to fcc phase. The deduced lattice parameters of both phases are in agreement with those of bulk alloys and experimental thin films.

Acknowledgements.

China Scolarship Council is acknowledged for grant #2009 60212.

References.

[1] J.-W. Yeh, Annales de Chimie - Science des Materiaux 31 (2006) 663.

[2] X. Yang and Y. Zhang, Materials Chemistry 132 (2012) 233-238

[3] U.S. Hsu, U.D. Hung, J.W. Yeh, S.K. Chen, Y.S. Huang, C.C. Yang, Materials Science and Engineering A 460–461 (2007) 403–408

[4] Chun-Ming Lin, Hsien-Lung Tsai, Intermetallics 19 (2011) 288-294

[5] Jien-Min Wu, Su-Jien Lin, Jien-Wei Yeh, Swe-Kai Chen, Yuan-Sheng Huang, Hung-Cheng Chen, Wear 261 (2006) 513–519

[6] J.-W. Yeh, S.-K. Chen, J.-Y. Gan, T.-S. Chin, T.-T. Shun, C.H. Tsau, S.-Y. Chan, Advanced Engineering Materials 6 (2004) 299.

[7] H.-W. Chang, P.-K. Huang, J.-W. Yeh, A. Davison, C.-H. Tsau, C.-C. Yang, Surface and Coatings Technology 202 (2008) 3360.

[8] M.-H. Tsai, Ji-W. Yeh, J.-Y. Gan, Thin Solid Films 516 (2008) 5527.

[9] T.-K. Chen, M.-S. Wong, T.-T. Shun, J.-W. Yeh, Surface and Coatings Technology 200 (2005) 1361.

[10] T.K. Chen, T.T. Shun, J.W. Yeh, M.S. Wong, Surface and Coatings Technology, 188–189 (2004) 193.

[11] V. Dolique, A.-L. Thomann, P. Brault, Y. Tessier, P. Gillon, Materials Chemistry and Physics 117 (2009) 142

[12] V. Dolique, A.-L. Thomann, P. Brault, Y. Tessier, P. Gillon, Surface & Coatings Technology 204 (2010) 1989

[13] S. J. Plimpton and A. P. Thompson, MRS Bulletin, 37(2012). 513-521

[14] H. J. C Berendsen.; J. P. M. Postma, W. F. van Gunsteren, A. DiNola, J. R. Haak, Journal of Chemical Physics 81 (1984). 3684

[15] Daw M S, Foiles S M and Baskes M I Mater. Sci. Reports 9 (1993) 251–310

[16] X. W. Zhou, R. A. Johnson and H. N. G. Wadley, Physical Review B 69 (2004) 144113

[17] D. B. Graves, P. Brault, J. Phys. D 42 (2009) 194011

[18] H. Balamane, T. Halicioglu, W. Tiller, Physical Review B, 46 (1992) 2250

[19] L. Z. Zhan, S. Y. Jiang, J. Chem. Phys. 117 (3002) 22

[20] L. Gang et al. Chin. Phys. Lett., 14 (1997) 764

[21] P. Brault, G. Moebs, Eur. Phys. J. AP 28 (2004) 43

[22] S.-W. Kao, J.-W. Yeh, T.-S. Chin, Journal of Physics: Condensed Matter, 20 (2008) 145214.

[23] C.C. Tung, J.-W. Yeh, T.-T. Shun, S.-K. Chen,Y;-S. Huang, H.-C. Chen, Materials Letters 61 (2007) 1

[24] W.-R. Wang, W.-L. Wang, S.-C. Wang, Y.-C. Tsai, C;-H. Lai, J.-W. Yeh, Intermetallics 26 (2012) 44

.

Table Captions

Table 1: LJ potential parameters σ and ε for Al, Co, Cr, Cu, Fe, Ni and Si

Species	ε(eV)	σ(Å)
Al	0.392	2.620
Co	0.510	2.306
Cr	0.502	2.336
Cu	0.409	2.338
Fe	0.527	2.321
Ni	0.520	2.282
Si	0.0175	3.826

Table 2: Simulated deposited alloy composition

Atoms	Al	Co	Cu	Cr	Fe	Ni
Deposited number	1309	1205	1293	1357	1348	1354
Sticking coefficient	0.78	0.72	0.77	0.81	0.81	0.81

Table 3: Average neighbour distances in the HEA compared to element crystal values.

Elements	Lattice parameter (Å)	1st neighbour (Å)	2nd neighbour (Å)	3rd neighbour (Å)	4th neighbour (Å)
Al (fcc)	a_{Al}= 4.05	$\frac{a_{Al}}{\sqrt{2}}$ = 2.86	a_{Al} = 4.05	$\sqrt{\frac{3}{2}}\,a_{Al}$= 4.96	$\sqrt{2}\,a_{Al}$= 5.73
Co (hcp)	a_{Co} = 2.51 c_{Co} = 4.07	a_{Co} = 2.51	$\sqrt{2}\,a_{Co}$ = 3.09	c_{Co} = 4.07	$\sqrt{2}\,c_{Co}$ = 5.76
Cu (fcc)	a_{Cu}= 3.61	$\frac{a_{Cu}}{\sqrt{2}}$ = 2.55	a_{Cu} = 3.61	$\sqrt{\frac{3}{2}}\,a_{Cu}$= 4.42	$\sqrt{2}\,a_{Cu}$= 5.10
Cr (bcc)	a_{Cr} = 2.88	$\frac{\sqrt{3}}{2}a_{Cr}$= 2.49	a_{Cr} = 2.88	$\sqrt{2}\,a_{Cr}$ = 4.07	$\sqrt{\frac{11}{4}}\,a_{Cr}$ = 4.78
Fe (bcc)	a_{Fe} = 2.87	$\frac{\sqrt{3}}{2}a_{Fe}$= 2.49	A_{Fe} = 2.87	$\sqrt{2}\,a_{Fe}$ = 4.06	$\sqrt{\frac{11}{4}}\,a_{Fe}$ = 4.76
Ni (fcc)	a_{Ni}= 3.52	$\frac{a_{Ni}}{\sqrt{2}}$ = 2.49	a_{Ni} = 3.52	$\sqrt{\frac{3}{2}}\,a_{Ni}$= 4.31	$\sqrt{2}\,a_{Ni}$= 4.98
Average	-	2.56	3.34	4.32	5.19
HEA T = 300 K	-	2.47	-	4.32	4.81
HEA T = 1095 K	-	2.47	-	-	4.60
HEA T = 1235 K	-	2.47	-	-	4.62
HEA T = 1500 K	-	2.467	-	-	4.61

Table 4: Experimental and calculated lattice parameters a. $2d_{hkl}\sin(\theta) = \lambda$ (1.54 Å) and $d_{hkl} = \frac{a}{\sqrt{h^2+k^2+l^2}}$.

Lattice parameters a	Bulk (calculated) [21,22]	Experiment thin films [12]	Present work
fcc phase	3.60 Å	300 K 3.66 Å 1100 K 3.64 Å	300 K 3.64 Å
bcc phase	2.86 Å	300 K 2.86 Å 1100 K none	1100 K 2.89 Å

Figure captions

Figure 1: Side and top views of snapshot of the simulated deposited HEA film. ●Al, ●Co, ●Cr, ●Cu, ●Fe, ●Ni, ●Si

Figure 2: Evolution of the total root mean square displacement against the temperature at various annealing rates.

Figure 3: Evolution of the total root mean square displacement against the temperature with second annealing method at various annealing rates.

Figure 4: The comparison of the total root mean square displacement against the temperature between the two annealing methods at the lowest annealing rates.

Figure 5: Successive snapshots of simulated annealing process at different temperatures. ●Al, ●Co, ●Cr, ●Cu, ●Fe, ●Ni, ●Si

Figure 6: Trajectory of typical Fe atom during annealing. Each point of the trajectory is separated by 2.5 K i.e.10 ps

Figure 7: Total RDF of the HEA deposit at different annealing temperatures.

Figure 8: The simulated XRD patterns at different annealing temperatures. The two tags at 43 and 45° refer to the experimentally observed fcc and bcc peak values [3].